IEEE Journal of Emerging and Selected Topics in Industrial Electronics, Vol. 3, No. 3, pp. 432-442, July 2022.

Impedance Compressing Matching Network Based on Two-Port Network Analysis for Wireless Power Transfer System

Euihoon Chung, *Student Member, IEEE,* Jung-Ik Ha, *Fellow, IEEE,*
Anas Al Bastami, *Student Member, IEEE,* and David J. Perreault, *Fellow, IEEE*

***Abstract*- This paper proposes a new design method of impedance matching networks for wireless power transfer systems. In wireless power transfer systems, the input impedance of resonator varies over a wide range rather than having a fixed value due to coupling variation. In conventional systems, tunable matching networks have been commonly used to match the variable impedance to a fixed impedance. Three-port impedance compression networks have also been proposed to eliminate the mechanical tuning processes. In this paper, a two-port impedance compressing matching network is proposed that addresses the load variations without the need for any mechanical tuning. In impedance matching, a two-port network can have a low design degree-of-freedom for load variation. In order to overcome this limitation, this paper analyzes the general model of a two-port network and proposes a systematic design procedure. The effectiveness of the proposed method is verified with a design example that constructs an Impedance Compressing Matching Network (ICMN).[1]**

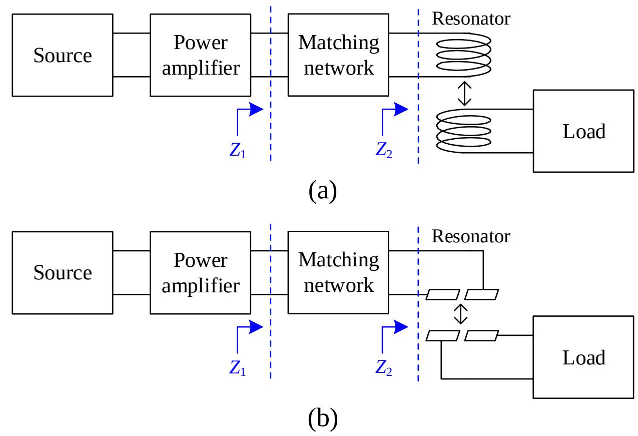

Fig. 1. Configuration of wireless power transfer systems (a) with inductive coupler, (b) with capacitive coupler.

I. Introduction

Wireless power transfer (WPT) is a technology that transfers energy from a transmitting side to a receiving side without any mechanical contact. With this convenience, the wireless power transfer technology has been adopted in various industrial applications such as smart phones, biomedical devices, home appliances, semiconductor processing equipment and electric vehicles [1, 2]. Fig. 1 shows a configuration of a typical wireless power transfer system. A power amplifier such as class D and class E amplifier synthesizes a high frequency AC waveform from a DC power source. The output of the power amplifier is connected to the resonator with a matching network. The AC power is transferred to the load through the resonator which is coupled in an inductive or a capacitive way as Fig. 1(a) and Fig. 1(b) respectively.

A performance of the power amplifier is highly dependent on the loading impedance denoted as Z_1 in Fig. 1. The power amplifier operates at the maximum efficiency with the minimal reflection loss at a specific loading condition (e.g., 50 Ω). On the other hand, the input impedance of the resonator denoted as Z_2 in Fig. 1 is usually not equal to the impedance desired by the power amplifier. In addition, the resonator impedance Z_2 varies over a wide range rather than having a fixed value. That is because the coupling of the resonator can vary depending on the misalignment or the condition of medium of the coupled resonators [3, 4]. Therefore, if the power amplifier and the resonator are directly connected to each other, the system is not only inefficient, but also very sensitive to coupling variation. Thus, the impedance matching network needs to be located between the power amplifier and the resonator, which provides the desired impedance transformation from Z_2 to Z_1. Also, the network needs to be carefully designed to achieve an acceptable impedance matching for a wide range of impedance variations [5, 6].

There have been several methods to design impedance matching systems considering the impedance variation. A typical method is to use a tunable matching network. Tunable matching networks include some variable reactance components such as Vacuum Variable Capacitors (VVC), switched capacitors, and varactors [7-12]. In a tunable matching network, the reactance of the tunable components is adjusted to compensate for load impedance variations. However, the use of tunable components increases the volume and cost of the system and increases the overall complexity. For example, for mechanical tuning of VVCs, some stepper motors and motor drive circuits need to be included. These motors and drive circuits are expensive and take large volumes in the system. In addition, mechanical tuning is extraordinarily slow and degrades the dynamic characteristics of the impedance matching process.

An alternative approach for impedance matching is to use multiple input or output ports networks without tunable components. For example, in [13-16], a three-port network

[1] This paper was presented in part at the Energy Conversion Congress and Exposition (ECCE), Baltimore, Maryland, USA, Sept.29-Oct.03, 2019.

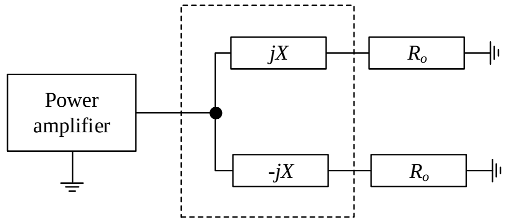

Fig. 2. Traditional three-port impedance compression network which requires two independent and identical loads.

called Impedance Compression Network (ICN) is used. Fig. 2 shows the typical structure of three-port ICN. The role of the ICN is to compress a matched set of widely-variable load impedances to a narrowly-varying impedance at its input port. This can provide improved matching to the cable and power amplifier such that the power amplifier always operates at the most efficient point. This method reduces the cost of the system and is especially useful if the load impedance varies rapidly and frequently. In [16], the ICN is used to compensate for misalignments in wireless power transfer system. However, as shown in Fig.2, the main disadvantage of using ICN is that it requires two independent and identical loads. Therefore, the implementation is more complicated than a two-port network with a single input port and a single output port.

There have also been several approaches to design two-port networks for resonant power conversion systems including wireless power transfer system. Most of them focused on listing all the possible network configurations based on the number of passive components and comparing their characteristics in order to select a network suited for a particular application [17-20]. These approaches are time-consuming and provide little intuition to designers. [21-23] presented a design method of a resonant network for wireless power transfer system considering a coupling variation. In order to obtain robust characteristics, the values of passive components constituting the resonant network were optimized with the network structure fixed. However, there was insufficient discussion on the criteria for selecting the structure of the network. In other words, there has been little explanation as to why such a network structure needs to be chosen to achieve the desired purpose.

This paper presents a new systematic modeling work of two-port networks. The goal of this work is to implement an impedance matching network that effectively compresses a single widely-varying load impedance without using tunable components or requiring multiple matched loads. This paper analyzes the general model of a two-port network and proposes a systematic design procedure. By defining design parameters from a general mathematical model of two-port network, it is possible to design a network that satisfied the desired input/output terminal properties without pre-determining a circuit structure. In this way, a circuit designer can systematically construct a network for their own purposes. This design process is fundamentally different from the previous method of optimizing the values of passive components with the circuit structure determined in advance.

Two-port networks can have low design degree-of-freedom for load variation. The feasibility and limitation of a fixed-frequency design method are discussed, and the authors show how variable-frequency operation over a narrow range can be

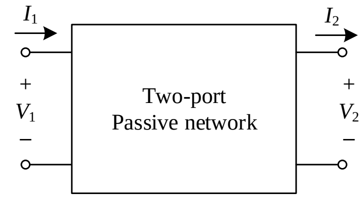

Fig. 3. The general model of the two-port network.

used to improve achievable performance. The two-frequency design method, which is the major contributing part of this paper, is proposed. The basic concept of the proposed design procedure has been presented in [24], which is the authors' conference paper. This paper extends the previous research [24] by providing a more detailed development of the modeling work and providing more experimental results for verification. The remainder of this paper is organized as follows. In Section II, the general perspective for interpreting a two-port network is introduced. In Section III, the two-frequency design method is proposed to construct a network that compresses load impedance variations. In Section IV, to show the effectiveness of this work, a two-port impedance compressing matching network (ICMN) is designed with the proposed method as a design example. In Section V, the detailed experimental results are presented for verification.

II. Analysis of Two-port Network Design

A two-port network represents a network having one input terminal and one output terminal, respectively. This paper analyzes a two-port network composed of only passive components. It is assumed that the reactance of each passive component is adjusted by an external circuit or device Fig. 3 describes a general two-port network model. Here, V_1 and I_1 are the voltage and the current of the input terminal, V_2 and I_2 are those of the output terminal. Then, the mathematical model of the two-port network is expressed as

$$\begin{bmatrix} V_1 \\ V_2 \end{bmatrix} = \begin{bmatrix} Z_{11} & Z_{12} \\ Z_{21} & Z_{22} \end{bmatrix} \begin{bmatrix} I_1 \\ -I_2 \end{bmatrix}. \tag{1}$$

If a two-port network consists of only passive components, the network is reciprocal. That is, in the impedance model, Z_{12} and Z_{21} always have the same value. Accordingly, the impedance model of the network is modified as follows

$$\begin{bmatrix} V_1 \\ V_2 \end{bmatrix} = \begin{bmatrix} Z_{11} & Z_{12} \\ Z_{12} & Z_{22} \end{bmatrix} \begin{bmatrix} I_1 \\ -I_2 \end{bmatrix}. \tag{2}$$

If their losses are negligible, the mathematical impedance model of the two-port network in (2) is simplified as follows

$$\begin{bmatrix} V_1 \\ V_2 \end{bmatrix} = \begin{bmatrix} jX_{11} & jX_{12} \\ jX_{12} & jX_{22} \end{bmatrix} \begin{bmatrix} I_1 \\ -I_2 \end{bmatrix}, \tag{3}$$

where X_{11}, X_{12}, and X_{22} are the imaginary part of Z_{11}, Z_{12}, and Z_{22}, respectively. Here, X_{11}, X_{12}, and X_{22} are only mathematical parameters and do not represent the impedance of a specific passive component yet. The network with the same mathematical parameters can be implemented in various ways. In subsection *A*, the meaning of X_{11}, X_{12}, X_{22} is elaborated, and the design freedom of two-port network is discussed. In subsection *B*, a method of constructing a circuit using these mathematical parameters is discussed.

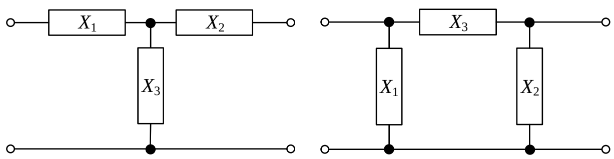

Fig. 4. Examples of circuit models: (a)T-model (b)Π-model.

A. Analysis on design variables of two-port network

The simplified impedance model of (3) implies the important fact that all the terminal properties of a two-port network such as input impedance (V_1/I_1) and voltage gain (V_2/V_1) are determined by only three parameters (X_{11}, X_{12}, X_{22}). Therefore, there are three degrees of freedom to determine terminal properties of a two-port network at an operating frequency. It is noted that the degree of freedom is independent of the number of passive components and is independent of how the network is structured. In this paper, three parameters (X_{11}, X_{12}, X_{22}) are selected as major design variables. In this way, a designer can define a two-port network that satisfies some desired input/output terminal properties without pre-determining the specific circuit configuration.

If the number of equations that constrain the terminal properties is defined as N_e and the degree of freedom is N_v, the possible design scenarios are classified into three cases as follows: (i) $N_e = N_v$, (ii) $N_e < N_v$, and (iii) $N_e > N_v$. In the cases of (i) and (ii), there may exist more than one candidate of design variables that satisfy the same desired terminal properties. In these cases, one among them can be chosen by defining some cost functions and evaluating each design candidate. On the other hand, in case (iii), there is no possible way to design a network to satisfy all the design constraints due to the lack of design freedom. In this case, no matter how much the number of passive components constituting the network is increased or how complicated the structure of the network is, the terminal properties are not satisfied.

Since the design variables X_{11}, X_{12}, and X_{22} are newly defined for each operating frequency, the only way to obtain new design freedom is to shift the operating frequency. For example, if a two-port network is designed based on two target frequencies, the design freedom increases to a maximum of six. Through frequency variation, a designer obtains the additional degree of freedom to satisfy more various terminal properties.

B. Implementation of two-port network as a circuit

As discussed in subsection *A*, the values of X_{11}, X_{12}, X_{22} at each target frequency are defined first. And then, a circuit is realized by selecting the combination of passive components to satisfy the values of X_{11}, X_{12}, X_{22}. As mentioned before, there are various ways to implement a network circuit having the same value of X_{11}, X_{12}, and X_{22}. In order to construct a circuit from design variables (X_{11}, X_{12}, X_{22}), a circuit model is needed. Fig. 4 shows the example of circuit models (a) T-model and (b) Π-model. In the T-model, for example, the relationship between the reactance of each branch (X_1, X_2, and X_3) and the design variables at an operating frequency are given as

$$\begin{cases} X_1 = X_{11} - X_{12}, \\ X_2 = X_{22} - X_{12}\,, \\ X_3 = X_{12}. \end{cases} \tag{4}$$

In the case of Π -model, the relationship is given as

$$\begin{cases} X_1 = \dfrac{X_{11}X_{22} - X_{12}^2}{X_{22} - X_{12}}, \\ X_2 = \dfrac{X_{11}X_{22} - X_{12}^2}{X_{11} - X_{12}}, \\ X_3 = \dfrac{X_{11}X_{22} - X_{12}^2}{X_{12}}. \end{cases} \tag{5}$$

Each branch having the desired reactance at a specific frequency (X_1, X_2, X_3) can be implemented in various form such as single passive component (inductor or capacitor), series connection of two passive components, and parallel connection of two passive components, and etc. If the reactance of each branch is defined at two or more frequencies, the circuit configuration that satisfies the values is more complicated. In Section III, the method to construct a branch in two frequency design is discussed in detail.

III. Impedance Compressing Matching Network Design

The input impedance of a network is one of the representative terminal properties. From (3) the relationship between Z_i and Z_o is determined by X_{11}, X_{12}, and X_{22} as

$$Z_i = jX_{11} + \frac{X_{12}^2}{Z_o + jX_{22}}, \tag{6}$$

where $Z_i = V_1/I_1$ and $Z_o = V_2/I_2$. Since Z_i and Z_o are complex numbers, (6) is divided into the real and the imaginary parts as

$$\begin{aligned} R_i &= \frac{X_{12}^2 R_o}{R_o^2 + (X_o + X_{22})^2}, \\ X_i &= X_{11} - \frac{X_{12}^2 (X_o + X_{22})}{R_o^2 + (X_o + X_{22})^2}, \end{aligned} \tag{7}$$

where R_o and X_o are the real, and the imaginary part of Z_o, and R_i and X_i are the real and the imaginary part of Z_i, respectively.

A. Limitation of the fixed frequency design

As shown in (7), two equations are required to transform a single load impedance to the desired input impedance. When the network is designed at one operating frequency, the number of equations (N_e) is two, and the degree of freedom (N_v) is three. Therefore, there exist many options to choose the design variables due to the one remaining degree of freedom. The design variables which ensure the single point impedance matching are calculated as

$$\begin{cases} X_{11} = X_i + mR_i, \\ X_{22} = -X_o + mR_o, \\ X_{12} = \pm\sqrt{(1 + m^2)R_o R_i}, \end{cases} \tag{8}$$

where *m* is an arbitrary real number that represents the remaining degree of freedom. In a single frequency design, due to lack of design freedom, it is impossible to match more than one load impedance to the desired input impedance as intended.

In many industrial fields such as wireless power transfer and plasma drive systems, the load impedance is variable rather than having a fixed value. In a single frequency design, the only way to consider the load impedance variation effect on input impedance is to change the value of *m*, which is the remaining degree of freedom. Previous research [25] has analyzed the effect of load resistance variation on the input impedance

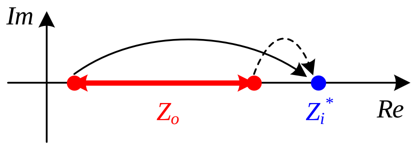

Fig. 5. A conceptual diagram of two end point impedance matching.

according to the value of m. However, the limitations of single-frequency design resulting from insufficient design freedom are also pointed out [26]. The limitations of a single-frequency design are discussed in more detail in Section IV.

B. Impedance compression with the two-frequency design

The key idea of the impedance compression method proposed in this paper is to first match the two endpoints of the load impedance variation range. Fig. 5 is a conceptual diagram of a method of matching two endpoints of the load impedance range (Z_o) to the specific point (Z_i^*). When both endpoints are matched, impedance compressing matching network (ICMN) can be easily realized by checking the continuity and optimizing the matching performance between them. However, in a fixed frequency design, only one load impedance can be matched as a designer intended. As mentioned in Section II, the only way to achieve additional design freedoms is to shift the operating frequency. At least two design frequencies are required because four equations need to be satisfied to match two endpoints of load impedance to the desired input impedance (e.g., 50 Ω). Therefore, this section introduces the simplest two-frequency design method.

In this section, it is assumed that a network is allowed to operate in a narrow frequency range f_s=[f_A, f_B]. In industrial fields, the allowable frequency tuning range of RF power generators is often about 5-10% [11, 14]. When the operating frequency range is determined, the network is designed at the two target frequencies: minimum and maximum frequencies (i.e., f_A and f_B).

There exist six degrees of freedom for two design frequencies as follows: [$X_{11,A}$, $X_{12,A}$, $X_{22,A}$] and [$X_{11,B}$, $X_{12,B}$, $X_{22,B}$] where subscripts A and B represent target frequencies. The design goal is to find the network to achieve sufficiently low reflection power for the whole load range by using the six available design variables. However, sweeping all the six parameters is a time consuming and non-intuitive process. Therefore, as mentioned earlier, the two endpoints matching method is suggested as an initial design. It means that the two endpoints of the load impedance range (Z_o=[$Z_{o,A}$, $Z_{o,B}$]) are preferentially matched to the desired values at each target frequency: (i) from $Z_{o,A}$ to $Z_{i,A}$ at f_A and (ii) from $Z_{o,B}$ to $Z_{i,B}$ at f_B. For the two endpoints impedance matching, the following equations need to be satisfied.

$$\begin{aligned} R_i^* &= \frac{X_{12,N}^2 R_{o,N}}{R_{o,N}^2 + \left(X_{o,N} + X_{22,N}\right)^2}, \\ X_i^* &= X_{11,N} - \frac{X_{12,N}^2\left(X_{o,N} + X_{22,N}\right)}{R_{o,N}^2 + \left(X_{o,N} + X_{22,N}\right)^2}, \end{aligned} \tag{9}$$

where subscript N is either A or B. From (8) and (9), the design variables ([$X_{11,A}$, $X_{12,A}$, $X_{22,A}$] and [$X_{11,B}$, $X_{12,B}$, $X_{22,B}$]) which ensure the two endpoints impedance matching are expressed as

$$\begin{cases} X_{11,N} = X_{i,N} + m_N R_{i,N}, \\ X_{22,N} = -X_{o,N} + m_N R_{o,N}, \\ X_{12,N} = \pm\sqrt{(1+m_N^2) R_{o,N} R_{i,N}}. \end{cases} \tag{10}$$

As shown in (10), there remain two degrees of freedom (m_A and m_B). Therefore, by adjusting the values of m_A and m_B, some design variables that ensure the two endpoints matching are collected. In this paper, the collected design variables that ensure the two endpoints matching are called as 'design candidates'.

In order to check the matching performance for the whole load impedance range between the two endpoints, each design candidate calculated by (10) needs to be implemented in an actual circuit. In this paper, it is assumed that the circuit is realized through the T-model. From (4), each branch needs to be configured to satisfy the following equations at two design frequencies.

$$\begin{cases} X_{1,N} = X_{11,N} - X_{12,N}, \\ X_{2,N} = X_{22,N} - X_{12,N}, \\ X_{3,N} = X_{12,N}, \end{cases} \tag{11}$$

where $X_{i,N}$ represents the reactance of each branch (i=1,2,3) at the frequency f_N. Each branch can be realized by one passive component (L or C) if the relationship of $X_{i,A}$ and $X_{i,B}$ is given by

$$\begin{aligned} k_x &= k_f \;\; (X_{i,A} > 0, X_{i,B} > 0), \\ k_x &= \frac{1}{k_f} \;\; (X_{i,A} < 0, X_{i,B} < 0), \end{aligned} \tag{12}$$

where k_f and k_x are defined as the ratio of the two target frequencies (k_f=f_B/f_A) and reactance at each frequency (k_x=$X_{i,B}$/$X_{i,A}$). In many cases, each branch is implemented with more than one passive component. If a branch consists of two passive components (LC series or parallel circuit), the possible impedance curves over the frequency range are shown in Fig. 5. Fig. 6(a), (c), and (e) show the cases where an LC series circuit forms a branch. Fig. 6(b), (d), and (f) show the cases where LC parallel circuit forms a branch. Then, the possible relationships of k_f and k_x are given as

$$\begin{aligned} k_x &< \frac{1}{k_f} \;\; (X_{i,A} < 0, X_{i,B} < 0), \\ k_x &> k_f \;\; (X_{i,A} > 0, X_{i,B} > 0), \\ &X_{i,A} X_{i,B} < 0. \end{aligned} \tag{13}$$

Other cases, which are not included in (12) and (13), can be realized by three or more passive components. In this paper, the number of passive components in each branch is limited to 2 or less in order to limit the total number of passive components included in the network. In other words, each branch is formed into one of L, C, LC series, or LC parallel circuit. Fig. 7 shows one example of the possible circuit configuration which has an LC series circuit in the 1st and 2nd branches and an LC parallel circuit in the 3rd branch. In this paper, this configuration of the network is defined as S/P/S (which means Series/Parallel/Series). Through the above circuit implementation process, each design candidate is realized as a 'circuit candidate'.

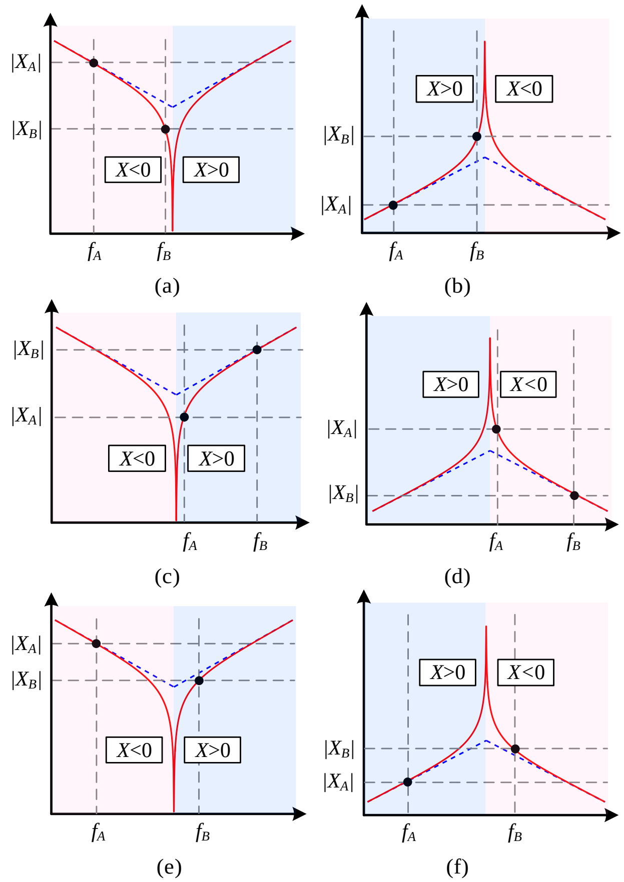

Fig. 6. Impedance curve according to the frequency of LC series (a),(c),(e) or LC parallel branch (b),(d),(f).

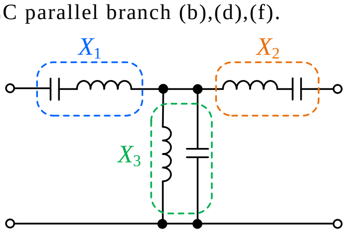

Fig. 7. One example of the possible network circuits which have the LC series circuit in the first and the second branches and the LC parallel circuit in the third branch (S/P/S).

Once the circuit candidates are implemented, the input impedance depending on frequency and the load impedance can be calculated. Then, the magnitude of the reflection coefficient ($|\Gamma|$) is calculated as follows

$$g = |\Gamma| = \left|\frac{Z_i(f_s, Z_o) - Z_i^*}{Z_i(f_s, Z_o) + Z_i^*}\right|. \tag{14}$$

Fig. 8 shows an example of $|\Gamma|$ in the three-dimensional plane depending on the frequency (f) and the load impedance (Z_o). Here, the red trajectory represents the set of $|\Gamma|$ minimized by the optimal frequency for each load impedance condition.

The next step is to define cost functions (g) to select one circuit among several circuit candidates. The matching performance for the whole impedance range can be evaluated by either the average or worst value of $|\Gamma|$ in (14). In addition, designers can consider some additional cost functions suitable for their design objectives. For example, the sum of maximum stored energy per unit power (kVA/kW rating) has been usefully adopted to

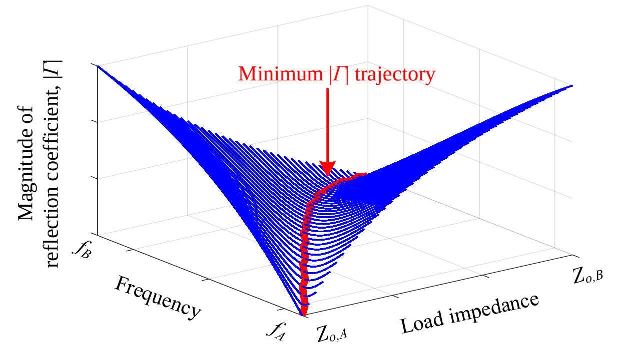

Fig. 8. An example of a 3-D plot representing the magnitude of reflection coefficient according to the frequency and the load impedance and the minimum reflection coefficient trajectory.

optimize the network volume and loss of a resonant network [26-28]. The index is calculated as

$$g = \frac{\Sigma|X_{Ln}||I_{Ln}|^2 + \Sigma|X_{Cn}||I_{Cn}|^2}{P_i}. \tag{15}$$

If there are more than two cost functions to be considered, there may be Pareto optimal points in which one cost cannot be reduced without increasing the other cost [29]. In that case, it is reasonable to select one circuit among Pareto optimal points.

IV. DESIGN EXAMPLE

A. *Resistance Compressing Matching Network (RCMN)*

In this section, a Resistance Compressing Matching Network (RCMN) is designed through the proposed network design procedure. The resistance compression means that an almost constant input resistance is achieved on the input side even when the resistive load varies over a wide range. The concept of the resistance compression has been usefully adopted in wireless power transfer system. In order to achieve the resistance compression characteristics, a three-port network using matched loads (termed Resistance Compression Networks, RCN) have been previously used [13-15]. The proposed RCMN differs from RCN in that it is implemented as a two-port network. Therefore, it requires a single load rather than two matched loads.

The range of load impedance (Z_o) depends on the application. Therefore, the range of Z_o needs to be determined considering the characteristics of the target system. In this design example, it is assumed that the resistive load impedance varies in the range of Z_o=[10 Ω, 40 Ω]. In this paper, the objective of the network design is to keep the input impedance as close to 50 Ω as possible. This is because it is important to match the input impedance to 50 Ω to minimize reflection loss in RF power systems. Here, the matching performance is evaluated by the magnitude of the reflection coefficient ($|\Gamma|$). The limit of $|\Gamma|$ allowed in the existing literature is 0.2 to 0.33. Based on this, in this paper, the maximum allowable value of $|\Gamma|$ is determined as 0.2 (i.e., $|\Gamma|$<0.2, corresponding to reflected power being less than 4%).

If the network is operated at a fixed frequency, only one load point can be transformed to the desired input impedance (50 Ω) as intended. In this example, it is assumed that the midpoint of the load range (20 Ω) is matched to 50 Ω. This is quite reasonable since the design goal is to minimize the worst value of $|\Gamma|$. The design variables that ensure the single point matching

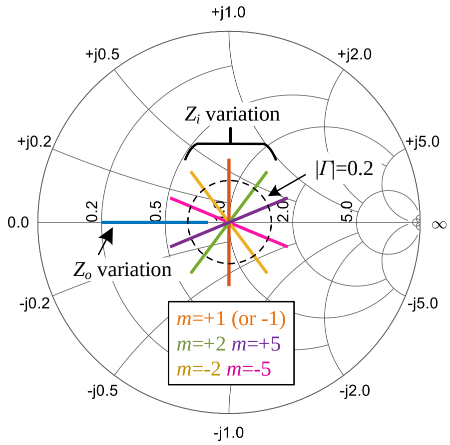

Fig. 9. Smith chart of single frequency design for RCMN.

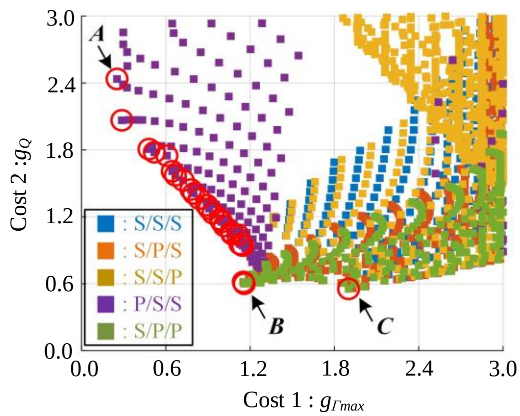

Fig. 10. Cost distribution of circuit candidates and Pareto optimal points determined by Cost 1 and Cost 2. Circuit *A* achieve the lowest value of Cost 1 but has the highest value of Cost 2. Circuit C achieve the highest value of Cost 1 but has the lowest value of Cost 2. Circuit B has the value of Cost 2 similar to that of Circuit C, but has a much smaller value of Cost 1 than Circuit A.

(from Z_o=20 Ω to Z_i=50 Ω) are determined by (8). Fig. 9 shows the Z_i variation according to the Z_o variation for different *m*. As shown in the figure, the worst value of $|\Gamma|$ is always the same and unacceptably high for all possible cases. This result shows the limitation of a fixed frequency design.

In order to achieve better matching performance, the network is designed based on the proposed two frequency design method. Here, the center frequency is determined as 13.56MHz, and it is assumed that ±5% narrow frequency tuning is allowed. Then, the operating frequency range is determined as f=[12.88MHz, 14.24MHz] (f_A=12.88MHz and f_B=14.24MHz).

As discussed in Section III, the degrees of design freedom ([$X_{11,A}$, $X_{12,A}$, $X_{22,A}$] and [$X_{11,B}$, $X_{12,B}$, $X_{22,B}$]) are initially utilized to provide two endpoints matching (from $Z_{o,A}$=10Ω to $Z_{i,A}$=50Ω at 12.88MHz and from $Z_{o,B}$=40Ω to $Z_{i,B}$=50Ω at 14.24MHz respectively). The design variables to ensure the two endpoints matching are calculated by (10). By adjusting the design freedoms m_A and m_B, several design candidates are obtained, and they can be implemented in circuit form by (11).

In order to evaluate circuit candidates, two cost functions ($g_{\Gamma max,N}$ and $g_{Q,N}$) are defined. The first one ($g_{\Gamma max,N}$) is the worst value of $|\Gamma|$ normalized by its base value 0.1, and the other ($g_{Q,N}$) is (kVA/kW) rating normalized by its base value 40. The meaning of the two cost functions was discussed in Section III.

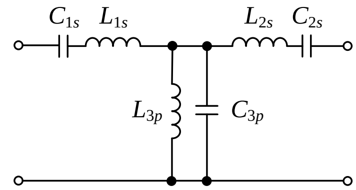

Fig. 11. The selected circuit configuration for two-port RCMN.

TABLE I THE VALUE OF PASSIVE COMPONENTS FOR THE SELECTED CIRCUIT IN DESIGN EXAMPLE A

Components	Value [Unit]
L_{1s}	1.05 [uH]
L_{2s}	2.58 [nH]
L_{3p}	69.3 [nH]
C_{1s}	110 [pF]
C_{2s}	521 [pF]
C_{3p}	1.65 [nF]

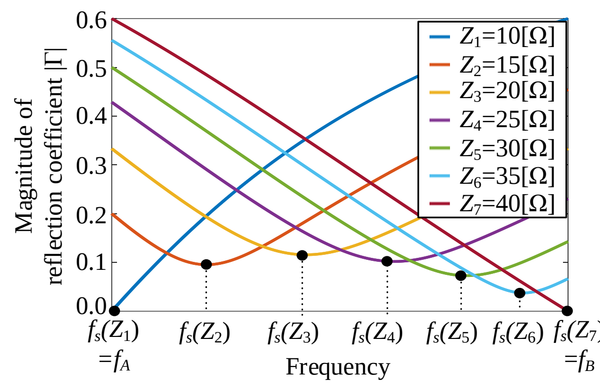

Fig. 12. The magnitude of the reflection coefficient according to the different load impedance conditions.

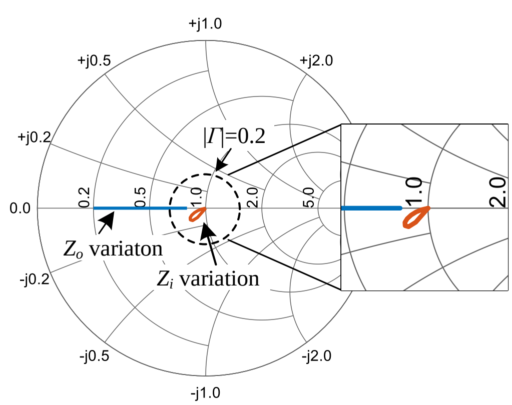

Fig. 13. Output impedance (Z_o) and corresponding input impedance (Z_i) estimated by simulation in design example A

Fig. 10 shows the cost distribution of more than 10,000 circuit candidates, which are generated by a grid-searching algorithm. Here, the circuits are grouped by their circuit configuration. For example, the circuit group named S/P/S has an LC series circuit in the 1st and the 2nd branches and an LC parallel connection in the 3rd branch. In Fig. 10, Pareto optimal points in which one cost cannot be reduced without increasing the other cost are marked as red circles. Obviously, it is reasonable for a designer to choose a circuit among Pareto optimal points. Comparing the three circuits circuit candidates *A*, *B*, and *C*, circuit candidate *A* has the lowest value of Cost 1, but the circuit is not desirable in

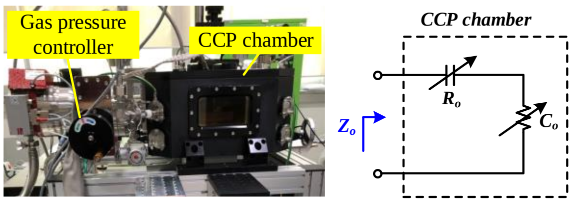

Fig. 14. (a) Photography and (b) equivalent circuit of CCP chamber.

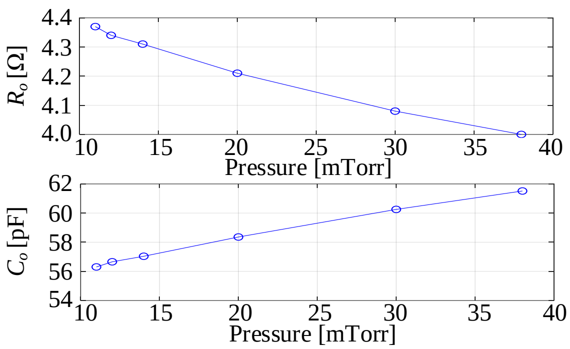

Fig. 15. The measured resistance and capacitance of CCP load according to gas pressure condition.

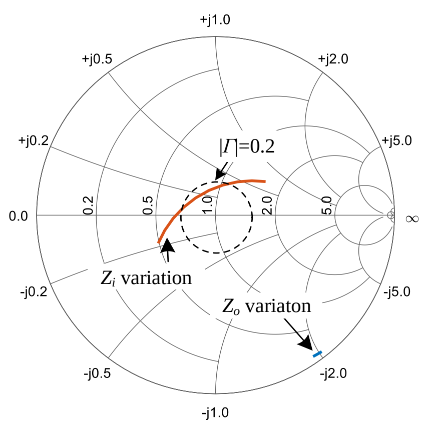

Fig. 16. Smith chart of single frequency design for ICMN in example B.

terms of Cost 2. Circuit candidate *C* has the lowest value of Cost 2, but the value of Cost 1 is higher than other circuit candidates. In the case of circuit candidate *B*, the value of Cost 2 is similar to that of circuit candidate *C*, but it has a much smaller value of Cost 1. The final decision on which of the Pareto optimal points to choose depends on the priority of cost functions determined by a designer.

The configuration of the selected circuit is shown in Fig. 11, and the values of the passive components for the circuit are listed in Table I. Fig. 12 shows the magnitude of the reflection coefficient ($|\Gamma|$) over frequency while varying the load impedance (Z_k). As intended in the design, $|\Gamma|$ is zero at both end load impedances ($Z_{o,A}$ = 10 Ω and $Z_{o,B}$ = 40 Ω). Also, only one optimal frequency appears to minimize $|\Gamma|$ for each load impedance condition. Thus, in the steady-state, the circuit operates at the frequency to minimize $|\Gamma|$ for each load condition. Fig. 13 shows the behavior of the input impedance Z_i according to the load impedance variation Z_o on the Smith chart. Here, the blue line represents the variation of Z_o, and the orange line represents the variation of the input impedance Z_i according to

TABLE II The value of passive components for the selected circuit in design example B

Components	Value [Unit]
L_{1s}	459.2 [nH]
L_{2s}	480.7 [nH]
L_{3p}	133.5 [nH]
C_{1s}	846.3 [pF]
C_{2s}	553.5 [pF]
C_{3p}	114.2 [pF]

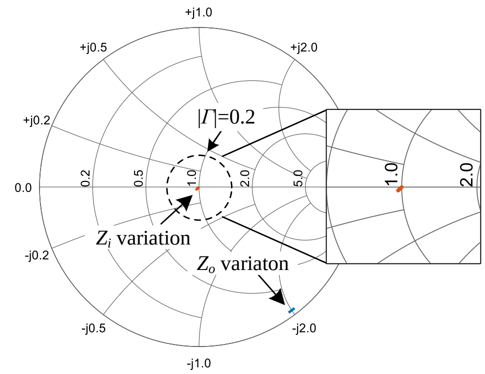

Fig. 17. Output impedance (Z_o) and corresponding input impedance (Z_i) estimated by simulation in design example B.

the load impedance variation. The black dotted circle indicates the maximum allowable value of $|\Gamma|$ ($|\Gamma|$=0.2). The simulation results show that the 400% load impedance variation is compressed within the $|\Gamma|$ allowable boundary. In this circuit, the maximum value of $|\Gamma|$ is 0.12, and the average value of $|\Gamma|$ is 0.06. Compared with the results in Fig. 9, which was achieved with a fixed frequency design over the same load impedance variation range, the narrow frequency variation of ±5% yields much better impedance compression performance.

B. Impedance Compressing Matching Network (ICMN)

In the second design example, a capacitively coupled plasma (CCP) drive system is introduced to prove the validity of the proposed method in industrial WPT application. The CCP drive system is a representative example of DC to AC wireless power transmission using capacitive coupler. In the CCP drive system, the high frequency electric field is generated by two electrodes installed in a gas-injected chamber, and the wirelessly transferred energy is applied to the load to generate plasma.

In this system, it is widely known that the equivalent load impedance depends on the gas pressure conditions. The range of the load impedance according to gas pressure is measured using the CCP chamber which is shown in Fig 14(a). The CCP load is modeled as a series connection of a resistor and a capacitor as shown in the Fig. 14(b). Fig. 15 shows the measured resistance R_o and capacitance C_o of the equivalent load model. The value of R_o decreases, and the value of C_o increases as the gas pressure increases from 10mTorr to 40mTorr. Based on these measurement results, the resistance variation range is defined R_o=[4.0 Ω, 4.4 Ω] and the capacitance variation range is defined C_o=[61.8 pF, 55.9 pF].

Fig. 16 shows the behavior of the input impedance Z_i according to the load impedance change Z_o when X_{11}, X_{12}, and X_{22} are optimized assuming that the operating frequency is fixed at 27.12MHz. As shown, the reflection factor exceeds the maximum allowable value (|Γ|=0.2) even if the network is

Fig. 18. RCMN prototype for experiments.

TABLE III TEST CONDITION AND MEASURED DATA IN EXAMPLE A

Test condition		Results	
Z_o [Ω]	f_s [MHz]	Z_i [Ω]	$\|\Gamma\|$
10	12.89	49.99+j0.866	0.009
12	12.98	48.11-j1.175	0.023
20	13.34	43.08-j4.551	0.089
25	13.56	41.79-j3.040	0.095
33	13.92	45.77-j0.216	0.044
40	14.24	46.80-j2.600	0.043

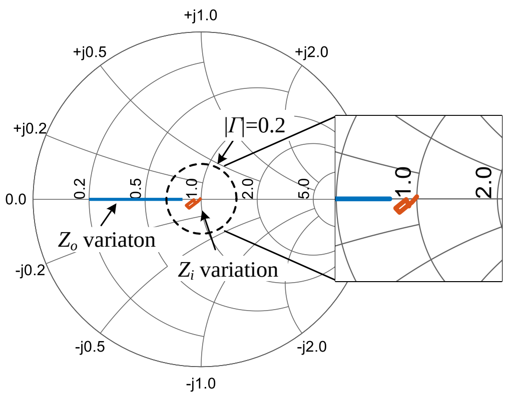

Fig. 19. Output impedance (Z_o) and corresponding input impedance (Z_i) measured by experiments in example A

optimized. This shows the limitation of the single frequency design for CCP drive system.

In order to achieve better impedance compressing performance, two frequency design method is applied again. It is noteworthy that in this example, unlike the previous example, the load is frequency dependent. However, the design process of ICMN is almost same. Here, the center frequency is selected as 27.12MHz, and it is assumed that ±2% narrow frequency tuning is allowed. Then, the operating frequency range is defined as f=[26.58MHz, 27.66MHz] (f_A=26.58MHz and f_B=27.66MHz). The degrees of design freedom ([$X_{11,A}$, $X_{12,A}$, $X_{22,A}$] and [$X_{11,B}$, $X_{12,B}$, $X_{22,B}$]) need to be selected to ensure two endpoints matching (from $R_{o,A}$=4.0Ω, $C_{o,A}$=61.8pF to $Z_{i,A}$=50Ω at 26.58MHz and from $R_{o,B}$=4.4Ω, $C_{o,B}$=55.9pF to $Z_{i,B}$=50Ω at 27.66MHz respectively). As in the previous example, by using the extra two degrees of freedom m_A and m_B, a lot of design candidates are generated. A designer selects one of the pareto optimal circuits. Since this process is described in the previous example, a detailed explanation of the design process is omitted in this subsection.

As a result, the S/P/S circuit is selected and its parameter values are listed in Table II. Fig. 17 shows output impedance (Z_o) and corresponding input impedance (Z_i) estimated by simulation. Compared with the single frequency design shown in Fig. 16, it is evident that the impedance compressing performance is highly improved through the two frequency design method.

TABLE IV TEST CONDITION AND MEASURED DATA IN EXAMPLE B

Test condition		Results	
Press.[mTorr]	f_s [MHz]	Z_i [Ω]	$\|\Gamma\|$
10	26.60	52.1-j3.40	0.039
17.5	27.05	53.2-j3.64	0.047
25	27.31	48.9-j0.39	0.012
34.5	27.49	48.9-j0.51	0.012
40	27.66	56.6-j2.92	0.068

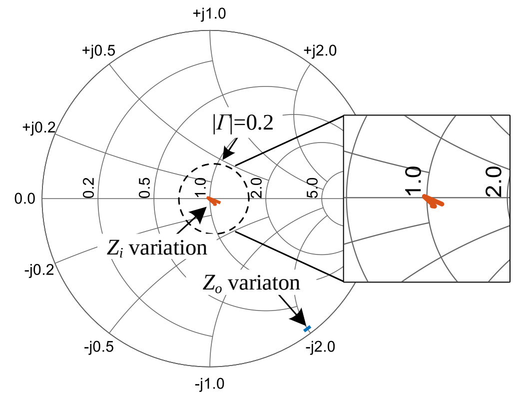

Fig. 20. Output impedance (Z_o) and corresponding input impedance (Z_i) measured by experiments in example B

V. EXPERIMENTAL VERIFICATION

A. Resistance Compressing Matching Network (RCMN)

In this subsection, the performance of the RCMN designed in Section IV is experimentally verified. A photograph of the RCMN prototype board is shown in Fig. 18. The manufacturing tolerance of capacitors is within 2%. The tolerance of the inductor is negligible since the inductors are fine-tuned. Also, since no core material is used in the prototype, the effect of saturation on the current is not a concern. The performance of the RCMN prototype board is verified by measuring the prototype's input impedance Z_i with an impedance analyzer according to the load impedance Z_o. The input impedance Z_i for various load impedance condition is measured using the impedance analyzer (HP4194A). Here, the load impedance (Z_o) is adjusted in several steps from 10 Ω to 40 Ω. The operating frequency is manually adjusted using a function generator (AFG3102) to minimize $|\Gamma|$. The input impedance (Z_i) measured at each test condition and the calculated value of $|\Gamma|$ are given in Table III. As shown in Table II, the maximum value of $|\Gamma|$ is about 0.1, which is lower than the limit ($|\Gamma|$ = 0.2). Fig. 19 shows the experimental results of the variation in Z_i with the variation in Z_o. There is an acceptable agreement between experimental and simulation results shown in Fig. 13. Some differences between experimental and simulation results may be due to some parameter tolerances of passive components.

B. Impedance Compressing Matching Network (ICMN)

In this subsection, ICMN design for CCP drive system is validated by experimental results. The input impedance Z_i of the ICMN prototype is measured according to the load variation while increasing the gas pressure in the chamber from 10mTorr to 40mTorr. The operating frequency of ICMN is manually adjusted to minimize $|\Gamma|$ for each loading condition. Table IV shows the measured input impedance (Z_i) and the value of $|\Gamma|$ at

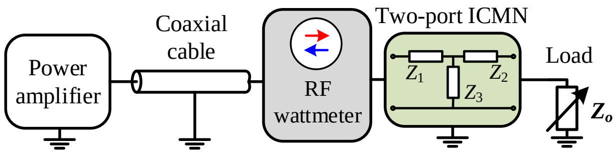

Fig. 21. Experimental setup using an RF wattmeter (Bird 43).

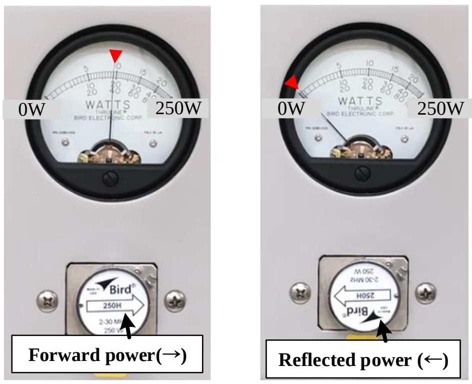

(a) (b)

Fig. 22. Power measurement: (a)forward power measurement and (b)reflected power measurement.

each test condition. As shown, the maximum value of $|\Gamma|$ is under 0.07, which is much lower than the limit ($|\Gamma|$ = 0.2). Fig. 20 shows the experimental results of the variation in Z_i according to variation in Z_o. Compared with the simulation results in Fig. 17, although some differences are observed due to errors in parameters and test conditions, the value of $|\Gamma|$ is still maintained at a low level inside the allowable range.

Fig. 21 shows an experimental setup using an RF wattmeter (Bird 43). RF wattmeter is inserted between the class E inverter and the ICMN prototype to measure the forward and reflected power. Fig. 22 shows the measurements of the forward and reflected power with the RF wattmeter in the worst case with the highest reflected power. The RF wattmeter is an analog instrument that measures the forward power or reflected power at a percentage (%) relative to the maximum measurable power of 250 W through the scale. Fig. 22(a) shows the forward power measurement mode and Fig. 22(b) shows the reflected power measurement mode. The results show that the forward power is about 100W, while the reflected power is measured close to 0W. The experimental results show that the impedance matching is performed well even when the power is supplied.

VI. CONCLUSION

This paper presents the modeling work of a two-port network and proposes the systematic design procedure to construct a two-port network that effectively compresses load impedance variations. The design method is based on a theoretical analysis of the two-port network. The feasibility and limitation of a fixed frequency design are discussed, and the two frequencies design method is proposed. As design examples, a two-port Resistance Compressing Matching Network (RCMN) for resistive load and Impedance Compressing Matching Network (ICMN) for frequency dependent load are constructed, and some experimental results are shown to verify the effectiveness of the design concept. For achieving better impedance matching performance, the frequency shifting technique is utilized in the two examples. In some applications where the load is sensitive to frequency variation, such as WPT system with a compensation topology, the operating frequency band needs to be carefully selected within a sufficiently narrow range to linearize the load variation. Network design with frequency range optimization is not the main scope of this paper, but it would be valuable if complemented by future work. The proposed modeling and design method is expected to be useful for designing networks robust to load impedance variation in various industrial fields including wireless power transfer system.

REFERENCES

[1] N. Shinohara, "Power without wires," *IEEE Microw. Mag.*, vol. 12, pp. S64-S73, 2011.

[2] V. J. Brusamarello, Y. B. Blauth, R. d. Azambuja, I. Muller, and F. R. d. Sousa, "Power Transfer With an Inductive Link and Wireless Tuning," *IEEE Trans. Instrum. Meas*., vol. 62, pp. 924-931, 2013.

[3] G. Notzon, T. Busch, M. v. Delden, and T. Musch, "A 500W high efficiency class-E power amplifier for heating a variable plasma load at 10MHz," in *Proc*. 12th German Microwave Conference (GeMiC), 2016, pp. 429-432.

[4] H. Feng, T. Cai, S. Duan, J. Zhao, X. Zhang, and C. Chen, "An LCC-Compensated Resonant Converter Optimized for Robust Reaction to Large Coupling Variation in Dynamic Wireless Power Transfer," *IEEE Trans. on Ind. Electron*., vol. 63, pp. 6591-6601, 2016.

[5] M. Liu, S. Liu, and C. Ma, "A High-Efficiency/Output Power and Low-Noise Megahertz Wireless Power Transfer System Over a Wide Range of Mutual Inductance," *IEEE Trans. on Microwave Theory and Tech.*, vol. 65, pp. 4317-4325, 2017.

[6] M. Liu, C. Zhao, J. Song, and C. Ma, "Battery Charging Profile-Based Parameter Design of a 6.78-MHz Class E2 Wireless Charging System," *IEEE Trans. on Ind. Electron.*, vol. 64, pp. 6169-6178, 2017.

[7] G. Bacelli, J. V. Ringwood, and P. Iordanov, "Impedance matching controller for an inductively coupled plasma chamber: L-type matching network automatic controller," *4th International Conference on Information in Control, Automation and Robotics*, 2007.

[8] T. C. Beh, M. Kato, T. Imura, S. Oh and Y. Hori, "Automated Impedance Matching System for Robust Wireless Power Transfer via Magnetic Resonance Coupling," in *IEEE Trans. on Ind. Electron.*, vol. 60, no. 9, pp. 3689-3698, Sept. 2013.

[9] H. M. Nemati, C. Fager, U. Gustavsson, R. Jos, and H. Zirath, "Design of varactor-based tunable matching networks for dynamic load modulation of high power amplifiers," in *IEEE Trans. Microw. Theory Tech.*, vol. 57,no. 5, pp. 1110–1118, May 2009.

[10] S. Aldhaher, P. C. Luk and J. F. Whidborne, "Tuning Class E Inverters Applied in Inductive Links Using Saturable Reactors," in *IEEE Trans. on Power Electron.*, vol. 29, no. 6, pp. 2969-2978, June 2014.

[11] A. S. Jurkov, A. Radomski, and D. J. Perreault, "Tunable impedance matching networks based on phase-switched impedance modulation," in *Proc. IEEE ECCE*, 2017, pp. 947-954.

[12] S. Liu, M. Liu, S. Han, X. Zhu and C. Ma, "Tunable Class E2 DC–DC Converter With High Efficiency and Stable Output Power for 6.78-MHz Wireless Power Transfer," in *IEEE Trans. on Power Electron*., vol. 33, no. 8, pp. 6877-6886, Aug. 2018.

[13] Y. Han, O. Leitermann, D. A. Jackson, J. M. Rivas and D. J. Perreault, "Resistance Compression Networks for Radio-Frequency Power Conversion," in *IEEE Trans. on Power Electron*., vol. 22, no. 1, pp. 41-53, Jan. 2007.

[14] A. Al Bastami et al., "Dynamic Matching System for Radio-Frequency Plasma Generation," in *IEEE Trans. on Power Electron*, vol. 33, no. 3, pp. 1940-1951, March 2018.

[15] W. Inam, K. K. Afridi and D. J. Perreault, "High Efficiency Resonant DC/DC Converter Utilizing a Resistance Compression Network," in *IEEE Trans. on Power Electron*., vol. 29, no. 8, pp. 4126-4135, Aug. 2014.

[16] J. Choi, J. Xu, R. Makhoul, and J. M. R. Davila, "Implementing an Impedance Compression Network to Compensate for Misalignments in a

Wireless Power Transfer System," in *IEEE Trans. on Power Electron.*, vol. 34, pp. 4173-4184, 2019.

[17] R. P. Severns, "Topologies for three-element resonant converters," in *IEEE Trans. on Power Electron.*, vol. 7, no. 1, pp. 89-98, Jan 1992.

[18] I. Batarseh, "Resonant converter topologies with three and four energy storage elements," in *IEEE Trans. on Power Electron.*, vol. 9, no. 1, pp. 64-73, Jan 1994.

[19] A. Khoshsaadat and J. S. Moghani, "Fifth-Order T-Type Passive Resonant Tanks Tailored for Constant Current Resonant Converters," in *IEEE Trans.* on *Circuits Syst. I: Reg. Papers*, vol. 65, no. 2, pp. 842-853, Feb. 2018.

[20] D. Huang, F. C. Lee, and D. Fu, "Classification and selection methodology for multi-element resonant converters," in *Proc. IEEE APEC*, 2011, pp. 558-565.

[21] M. Liu, S. Liu, and C. Ma, "A High-Efficiency/Output Power and Low-Noise Megahertz Wireless Power Transfer System Over a Wide Range of Mutual Inductance," IEEE Trans. on Microwave Theory and Tech., vol. 65, pp. 4317-4325, 2017.

[22] H. Feng, T. Cai, S. Duan, J. Zhao, X. Zhang, and C. Chen, "An LCCCompensated Resonant Converter Optimized for Robust Reaction to Large Coupling Variation in Dynamic Wireless Power Transfer," IEEE Trans. on Ind. Electron., vol. 63, pp. 6591-6601, 2016.

[23] J. Feng, M. Fu, Q. Li, and F. C. Lee, "Resonant converter with coupling and load independent resonance for omnidirectional wireless power transfer application," in Proc. IEEE ECCE, 2017, pp. 2596-2601.

[24] E. Chung, J. Ha, "Resonant network design methodology based on two-port network analysis considering load impedance variation," in *Proc IEEE ECCE*, 2019, to be published.

[25] E. Chung, G. C. Lim, J. Ha and D. J. Perreault, "Resonant Converter Design Using Two-Port Passive Network: Single Frequency Design," in *Proc IEEE COMPEL*, 2018, pp. 1-7.

[26] M. Danilovic, K. D. T. Ngo and Z. Zhang, "Compression of the load resistance range in constant frequency resonant inverters," in *Proc. IEEE ECCE*, 2014, pp. 2793-2800.

[27] K. Jalili and S. Bernet, "Design of LCL Filters of Active-Front-End Two-Level Voltage-Source Converters," in *IEEE Trans. on Ind. Electron.*, vol. 56, no. 5, pp. 1674-1689, May 2009.

[28] G. Zeng, T. W. Rasmussen, and R. Teodorescu, "A novel optimized LCL-filter designing method for grid connected converter," in Proc. *IEEE PEDG*, 2010, pp. 802-805.

[29] M. Borage, K. V. Nagesh, M. S. Bhatia and S. Tiwari, "Resonant Immittance Converter Topologies," in *IEEE Trans. on Ind. Electron.*, vol. 58, no. 3, pp. 971-978, March 2011.

[30] R. Bosshard, J. W. Kolar, J. Mühlethaler, I. Stevanović, B. Wunsch and F. Canales, "Modeling and η-α-Pareto Optimization of Inductive Power Transfer Coils for Electric Vehicles," in *IEEE JESTPE*, vol. 3, no. 1, pp. 50-64, March 2015.

Euihoon Chung (S'14) received the B.S. and Ph.D. degrees in electrical engineering from Seoul National University, Seoul, Korea, in 2014 and 2020 respectively.

His research interests are in design of dc-dc converters and high-frequency power conversion system including battery charging, wireless power transfer, and plasma drive systems.

Jung-Ik Ha (S'97–M'01–SM'12–F'18) received the B.S., M.S., and Ph.D. degrees in electrical engineering from Seoul National University, Seoul, Korea, in 1995, 1997, and 2001, respectively. From 2001 to 2002, he was a Researcher in Yaskawa Electric Co., Japan. From 2003 to 2008, he worked with Samsung Electronics Co., Korea, as a Senior and Principal Engineer. From 2009 to 2010, he was a Chief Technology Officer with LS Mecapion Co., Korea. Since 2010, he has been with the Department of Electrical and Computer Engineering, Seoul National University, Seoul, Korea, where he is currently a Professor. He is also with Seoul National University Electric Power Institute. From 2016 to 2017, he was a Visiting Scholar with Massachusetts Institute of Technology, MA, USA.

His research interests include circuits and control in high efficiency and integrated electric energy conversions for various industrial fields. Dr. Ha is an Associate Editor for IEEE Journal of Emerging and Selected Topics in Power Electronics and the Editor-in-Chief of Journal of Power Electronics.

Anas Al Bastami (S'10) received the B.S. degree from Texas A&M University at Qatar, Doha, Qatar, in 2012, and the S.M. degree in 2014 from the Massachusetts Institute of Technology (MIT), Cambridge, MA, USA, both in electrical engineering. He is currently working toward the Ph.D. degree in electrical engineering in the Laboratory for Electromagnetic and Electronic Systems, MIT.

His interests include engineering education, and research in the areas of circuit design, embedded systems, power electronics, and renewable energy systems. Since joining MIT, he has been conducting research in various areas of interest, including radio-frequency power amplifiers and converters, impedance matching systems, and high-performance power electronic systems for a wide range of applications.

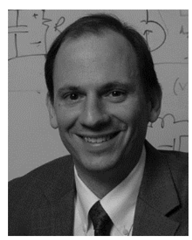

David J. Perreault (S'91–M'97–SM'06–F'13) received the B.S. degree from Boston University, Boston, MA, USA, in 1989, and the S.M. and Ph.D. degrees from the Massachusetts Institute of Technology, Cambridge, MA, USA., 1991 and 1997, respectively.

In 1997, he joined the MIT Laboratory for Electromagnetic and Electronic Systems as a Postdoctoral Associate and became a Research Scientist in the laboratory in 1999. In 2001, he joined the MIT Department of Electrical Engineering and Computer Science (EECS), Cambridge, where he is currently a Professor of electrical engineering. He has held multiple roles within the EECS Department, most recently as the Associate Department Head from 2013– 2016. His research interests include design, manufacturing, and control techniques for power electronic systems and components and their use in a wide range of applications. He also consults in industry, and co-founded Eta Devices, Inc., (acquired by Nokia in 2016) and Eta Wireless, Inc., startup companies focusing on high-efficiency RF power amplifiers.

Dr. Perreault received the Richard M. Bass Outstanding Young Power Electronics Engineer Award, the R. David Middlebrook Achievement Award, the ONR Young Investigator Award, and the SAE Ralph R. Teetor Educational Award, and is the co-author of eleven IEEE prize papers.